Quantum magnetotransport properties of silicene: Influence of the acoustic phonon correction

Hong T. T. Nguyen [1,2,*] Le Dinh,[3] Tuan V. Vu [1,2] Le T. Hoa [3] Nguyen N. Hieu [4,5,†] Chuong V. Nguyen,[6] Hieu V. Nguyen,[7] S. S. Kubakaddi [8] and Huynh V. Phuc [9,‡]

[1]*Division of Computational Physics, Institute for Computational Science, Ton Duc Thang University, Ho Chi Minh City 700000, Vietnam*
[2]*Faculty of Electrical and Electronics Engineering, Ton Duc Thang University, Ho Chi Minh City 700000, Vietnam*
[3]*Center for Theoretical and Computational Physics, University of Education, Hue University, Hue 530000, Vietnam*
[4]*Institute of Research and Development, Duy Tan University, Da Nang 550000, Vietnam*
[5]*Faculty of Natural Sciences, Duy Tan University, Da Nang 550000, Vietnam*
[6]*Department of Materials Science and Engineering, Le Quy Don Technical University, Hanoi 100000, Vietnam*
[7]*Department of Physics, The University of Da Nang, University of Science and Education, Da Nang 550000, Vietnam*
[8]*Department of Physics, K. L. E. Technological University, Hubballi 580 031, Karnataka, India*
[9]*Division of Theoretical Physics, Dong Thap University, Cao Lanh 870000, Vietnam*

(Received 9 January 2021; revised 6 June 2021; accepted 16 August 2021; published 24 August 2021)

We study the transport properties of silicene in a perpendicular magnetic field by evaluating the Hall and longitudinal conductivities and resistivities when the acoustic phonon correction to the Landau level (LL) energy is taken into account. The acoustic phonons are considered by three modes: the transverse (TA), longitudinal, and out-of-plane ones. Under the influence of the acoustic phonon correction, the quantum Hall effect plateaus occur at higher values of the magnetic field, where the TA phonon displays the strongest effect. The combined effects of the strong spin-orbit coupling in silicene, the external electric field, and the Zeeman field on the transport parameters are investigated. These combined effects lift the spin and valley degeneracy of the LLs, leading to the additional plateaus in the Hall conductivity with the sequence being found as $\sigma_{yx} = (4e^2/h)(n/4 + 1/2)$. The temperature has a significant effect on the width of the Hall conductivity plateaus. We also appraise the longitudinal conductivity σ_{xx} and the Hall, ρ_{xy}, and longitudinal, ρ_{xx}, resistivities and show the difference between the present results and those for graphene as well as for silicene without the Zeeman field effect. The combined effects of the electric and Zeeman fields lead to the quadrupled peaks of ρ_{xx} and the sequence of $(h/e^2)/(n + 2)$ in the height of the plateaus in ρ_{xy}.

DOI: 10.1103/PhysRevB.104.075445

I. INTRODUCTION

Silicene is a two-dimensional (2D) honeycomb monolayer of silicon [1], which has been predicted to be stable and argued to be one of the most competitive in the 2D materials family [2,3]. Having the same sheetlike structure as graphene, silicene has outstanding properties similar to those of graphene [4]. However, unlike in graphene, where the C atoms are bonded together to form a planar structure, in silicene, the Si atoms are also bonded together to form a honeycomb structure, but with a low buckled geometry caused by its large ionic radius size [2,5–8]. It means that the 2D silicene sheet is not a truly planar structure where the sublattices are located on different planes with a distance of $2d = 0.46$ Å [9,10]. This buckling in silicene awards the possibility for controlling its band gap by an electric field E_z [10–12]. In addition, silicene has been demonstrated to have a large intrinsic spin-orbit coupling (SOC) resulting in a gap of $\Delta_{SO} = 3.9$ meV [6]. In addition to the control of the band gap, the applied E_z is also predicted to control the transition phase in silicene [9,11–13]: At a small electric field value such that $\Delta_z < \Delta_{SO}$ ($\Delta_z = edE_z$ is associated with the staggered sublattice potential in the electric field [14]), the system displays a natural topological insulator (TI) phase. By increasing E_z such that $\Delta_z > \Delta_{SO}$, it shows a transition phase from the TI to the band insulator (BI). At the charge neutrality point ($\Delta_z = \Delta_{SO}$) silicene refers to a valley-spin-polarized metal (VSPM) phase. These features make silicene unique, which is advantageous in comparison with the zero-band-gap feature of graphene in the application to fabricate electronics devices. Therefore, silicene is expected to replace graphene to start a new era of tunable electronic devices. A recent study of the SOC gap in silicene predicted an experimentally observable Hall effect in the low-temperature region [5]. In another work, the combined effect of an electric field and intrinsic SOC was demonstrated to lead to phase transitions at the point of $\Delta_z = \Delta_{SO}$, which provides a useful way to experimentally adjust the topological state of silicene [15].

One of the most remarkable phenomena observed in the materials in the magnetic field is the quantum Hall effect (QHE) [16,17]. The original version is referred to as the integer QHE, where the Hall conductivity σ_{yx} takes on the quantized values of $(2e^2/h)(n + 1)$, with n, h, and e being an integer, Planck's constant, and the elementary charge, respectively. This is named conventional integer QHE. Thereafter, an expanded version, named unusual QHE, was discovered

*nguyenthithamhong@tdtu.edu.vn
†Corresponding author: hieunn@duytan.edu.vn
‡Corresponding author: hvphuc@dthu.edu.vn

in graphene [18,19], where the Hall conductivity takes values of $(4e^2/h)(n+1/2)$, which is completely different from conventional semiconductors. This observation is in agreement with that predicted by a theoretical study [20] in which the (2+1)-dimensional Dirac theory was used to describe the quasiparticle excitations in monolayer graphite films. The unusual QHE was also obtained in graphene in the case of zero Hall field [21]. In another work [22], using Kubo formulas, Krstajić and Vasilopoulos obtained analytical expressions for the Hall and longitudinal conductivities in gapped graphene. They also predicted a new plateau of the Hall conductivity at $n=0$ which was demonstrated to be the result of the existence of the finite band gap in gapped graphene. A similar result was observed in MoS_2 monolayer [23] and in silicene [24–26].

Motivated by the above discussions, in this work, we study the QHE in silicene where the electric and Zeeman fields are taken into account. It was demonstrated that the combined effect of electric and Zeeman fields makes the Landau levels (LLs) completely separate, or nondegenerate [27]. This separation results in an increase in the number of transitions compared to the absence of a Zeeman field [24–26]. Consequently, the new plateaus of the Hall conductivity are added with the sequence $\sigma_{yx}=(4e^2/h)(n/4+1/2)$. We also study the influence of the acoustic phonon correction on the LLs using the Migdal approximation [28–30]. The acoustic phonons are considered by three modes: the transverse (TA), longitudinal (LA), and out-of-plane (ZA) ones. While the correction due to impurity is small [21,22], the correction due to electron-acoustic phonons on the LLs was demonstrated to have a remarkable effect on the LLs spectrum [31–34]. Therefore, this correction is expected to have an essential influence on the quantum magnetotransport properties of elemental two-dimensional materials such as silicene. We also appraise the longitudinal conductivity σ_{xx} and the Hall, ρ_{xy}, and longitudinal, ρ_{xx}, resistivities and show the difference between the present results and those for graphene as well as for silicene ignoring the Zeeman field effect.

In Sec. II we briefly give the eigenfunctions and eigenvalues of electrons in silicene. The correction to the LLs due to electron-acoustic phonon scattering is shown in Sec. III. The evaluation of the relevant conductivities and resistivities is presented in detail in Sec. IV. Our summary is carried out in Sec. V. Finally, the energy corrections using first-order perturbation theory due to impurity and acoustic phonon interactions, the effect of electron concentration on the self-energy, and the Hall conductivity for a finite LL broadening are outlined in the Appendixes.

II. SILICENE IN AN EXTERNAL MAGNETIC FIELD

Consider a silicene sample in the (xy) plane with an area $\mathcal{S}_0=L_xL_y$. In the presence of a uniform magnetic field $\mathbf{B}=(0,0,B)$, the effective Hamiltonian of low-energy electrons, in the neighborhood of the K point, is given as follows [9,35]:

$$\mathcal{H}_0=v_{\rm F}(\tau\sigma_x\pi_x+\sigma_y\pi_y)+\Delta^z_{\tau,s}\sigma_z+sM_z, \tag{1}$$

where $v_{\rm F}=5.42\times10^5$ m/s is the Fermi velocity [6]; $\boldsymbol{\pi}=\mathbf{p}+e\mathbf{A}$ is the carrier momentum; $\mathbf{A}$ denotes the vector potential of the magnetic field; $\tau, s=\pm$ are the valley and spin indices, respectively; and σ_x, σ_y, and σ_z are the Pauli matrices. Also, $\Delta^z_{\tau,s}=\tau s\Delta_{\rm SO}-\Delta_z$, where $\Delta_z=edE_z$ is associated with the staggered sublattice potential in the electric field [14], and $M_z=e\hbar B/m_e$ is the Zeeman field part of the Hamiltonian, with $m_e=0.26m_0$ [36] being the electron effective mass, with m_0 being the free-electron mass. Using the gauge $\mathbf{A}=(0,Bx,0)$, the eigenvalues are found to be

$$E^{(0)}_\lambda\equiv E^{\tau,p(0)}_{n,s}=pE^\tau_{n,s}+sM_z. \tag{2}$$

Here, for $n\neq0$, $E^\tau_{n,s}=[(\Delta^z_{\tau,s})^2+n(\hbar\omega_c)^2]^{1/2}$, the cyclotron frequency $\omega_c=v_{\rm F}\sqrt{2}/\ell_c$, and $\alpha_c^2=\hbar/eB$. For $n=0$ the energy is $E^{\tau(0)}_{0,s}=-\tau\Delta^z_{\tau,s}+sM_z$. The symbol λ is denoted for $\{\xi,k_y\}$, i.e., $|\lambda\rangle=|\xi,k_y\rangle$, where ξ is used as shorthand for $\{n,s,\tau,p\}$. Here, the integer numbers n $(=0,1,2,\ldots)$ are the LL indices, and $p=\pm$ indicates the conduction $(p=+)$ and valence $(p=-)$ bands. The corresponding normalized eigenfunctions for the K valley $(\tau=+)$ are

$$\psi^{+,p}_{n,s}(\mathbf{r},k_y)=\frac{e^{ik_yy}}{\sqrt{L_y}}\begin{pmatrix}A^{+,p}_{n,s}\phi_{n-1}(X)\\ ipB^{+,p}_{n,s}\phi_n(X)\end{pmatrix}, \tag{3}$$

where $\mathbf{r}=(x,y)$ is the 2D position vector, $\phi_n(X)$ are the normalized harmonic oscillator eigenfunctions, and $X=(x-\alpha_c^2k_y)/\alpha_c$. The normalization coefficients $A^{\tau,p}_{n,s}$ and $B^{\tau,p}_{n,s}$ are given by

$$A^{+,p}_{n,s}=\sqrt{\frac{1+\chi^{+,p}_{n,s}}{2}},\quad B^{+,p}_{n,s}=\sqrt{\frac{1-\chi^{+,p}_{n,s}}{2}}, \tag{4}$$

where $\chi^{+,p}_{n,s}=\Delta^z_{+,s}/(pE^+_{n,s})$. The normalized eigenfunctions for the zeroth level are

$$\psi^{\tau=+}_0=\frac{e^{ik_yy}}{\sqrt{L_y}}\begin{pmatrix}0\\ i\phi_0(X)\end{pmatrix}. \tag{5}$$

The corresponding eigenfunctions for the K' valley $(\tau=-)$ are also given by Eqs. (3) and (5) but with the interchange between ϕ_n and ϕ_{n-1} and also $\Delta^z_{+,s}$ replaced by $-\Delta^z_{-,s}$.

III. CORRECTION TO THE LANDAU LEVELS DUE TO ELECTRON-ACOUSTIC-PHONON INTERACTION

When the carrier-phonon interaction is taken into account, due to this interaction, the energy levels of a carrier in silicene are modified [31–34], and the new spectrum can be written as

$$E_\lambda=E^{(0)}_\lambda+{\rm Re}\Sigma_\lambda, \tag{6}$$

where $E^{(0)}_\lambda$ denotes the unperturbed energy spectrum, ${\rm Re}(\cdots)$ denotes the real part of $(\cdots)$, and Σ_λ is the diagonal part of the electron self-energy operator, i.e., $\Sigma_\lambda=\langle\lambda|\Sigma(\mathbf{r},\mathbf{r}',E^{(0)}_\lambda)|\lambda\rangle$, with $\mathbf{r}$ and $\mathbf{r}'$ being the position vectors [37]. The term ${\rm Re}\Sigma_\lambda$ represents the change in the electron energy, which is treated within the Migdal approximation as follows [28–30]:

$${\rm Re}\Sigma_\lambda=\sum_{\lambda'\neq\lambda}\sum_{q,\zeta}|M^\zeta_{\lambda'\lambda}(q)|^2\left[\frac{N_{q,\zeta}+f\left(E^{(0)}_{\lambda'}\right)}{E^{(0)}_\lambda+\hbar\omega_{q,\zeta}-\left(E^{(0)}_{\lambda'}-\mu\right)}+\frac{N_{q,\zeta}+1-f\left(E^{(0)}_{\lambda'}\right)}{E^{(0)}_\lambda-\hbar\omega_{q,\zeta}-\left(E^{(0)}_{\lambda'}-\mu\right)}\right]. \tag{7}$$

Here, $N_{q,\zeta}=[\exp(\beta\hbar\omega_{q,\zeta})-1]^{-1}$ is the Bose distribution function for a phonon of wave vector $q=(q_x,q_y)$ and energy

TABLE I. Material parameters for silicene [39,41].

	ZA	TA	LA
$v_{s,\zeta}$ ($\times 10^3$ m/s)	0.63	5.4	8.8
D_a (eV)	2.0	8.7	3.2

$\hbar\omega_{q,\zeta}$, with ζ denoting the branch of phonon, $\beta = 1/(k_B T)$, and $f(E^{(0)}_{\lambda'}) = \{1 + \exp[\beta(E^{(0)}_{\lambda'} - \mu)]\}^{-1}$ is the Fermi distribution function for a carrier at energy $E^{(0)}_{\lambda'}$ and chemical potential μ. The matrix element for carrier-phonon interaction is given by [38]

$$\left|M^{\zeta}_{\lambda'\lambda}(q)\right|^2 = \left|g^{\zeta}_q\right|^2 |J_{\lambda'\lambda}(u)|^2 \delta_{k'_y, k_y \pm q_y}, \tag{8}$$

where g^{ζ}_q is the carrier-phonon coupling strength which depends on the phonon mode ζ and the form factor is given by

$$|J_{\lambda'\lambda}(u)|^2 = e^{-u} u^j \frac{k!}{(k+j)!}\left[B^{\tau,p}_{n,s} B^{\tau',p'}_{n',s'} L^j_k(u) + A^{\tau,p}_{n,s} A^{\tau',p'}_{n',s'} \sqrt{\frac{k+j}{k}} L^j_{k-1}(u)\right]^2. \tag{9}$$

Here, $u = \alpha_c^2 q^2/2$, $k = \min[n', n]$, $j = |n' - n|$, and $L^j_k(u)$ is the associated Laguerre polynomial. In this work, we consider the interaction between carriers with three different modes of acoustic phonons (ζ = ZA, TA, and LA). The corresponding electron-phonon coupling strength is [39]

$$\left|g^{\zeta}_q\right|^2 = \frac{\hbar D_a^2 q}{2\mathcal{S}_0 \rho v_{s,\zeta}}, \tag{10}$$

where $\rho = 7.6 \times 10^{-7}$ kg/m^2, D_a is the deformation potential constant, and $v_{s,\zeta}$ is the sound velocity [38,40].

The evaluation of $\mathrm{Re}\Sigma_\lambda$ in Eq. (7) needs a cutoff. As in the case of gapless graphene [33], here, we use a high-energy cutoff of $|E_{\rm cut}| = \sqrt{\pi\sqrt{3}t} \approx 2.49$ eV, corresponding to a LL cutoff $n_{\rm cut}$, which is the integer part of $(|E_{\rm cut}|/E^{+1(0)}_{1,1})^2$. Therefore, $n_{\rm cut}$ varies roughly as $1.6 \times 10^4/(B[\mathrm{T}])$.

Figure 1(a) shows the dependence of the real part of the exchange self-energy for $n = 0$ on the magnetic field. We can see that it is independent of the magnetic field. This feature is true not only for the zero level, as shown in Fig. 1(a), but also for all other LLs. For each valley K and K', the addition of the energy gap due to acoustic phonon interaction is determined by the difference between $\mathrm{Re}\Sigma_\lambda(s = +1)$ and $\mathrm{Re}\Sigma_\lambda(s = -1)$; therefore, the addition of the energy gap is independent of the magnetic field, in agreement with that due to SO-phonon scattering in graphene [42]. For the contribution of each branch of acoustic phonons, with the smallest value of the ratio D_a^2/v_s^{ζ} (see Table I) the LA phonon gives the smallest contribution to the retarded self-energy, followed by that of the ZA phonon, and the TA phonon exhibits the strongest one. The total energy correction due to the acoustic phonon to the zero level is about $0.97\Delta_{\rm SO}$, equivalent to 3.77 meV. This value is comparable to that due to impurity scattering (see Sec. A 1) but much larger than that due to acoustic phonon scattering (see Sec. A 2) using the first-order perturbation theory at $B = 5$ T. To our knowledge, there are no experimental data for the phonon correction in silicene. However, these experimental data have

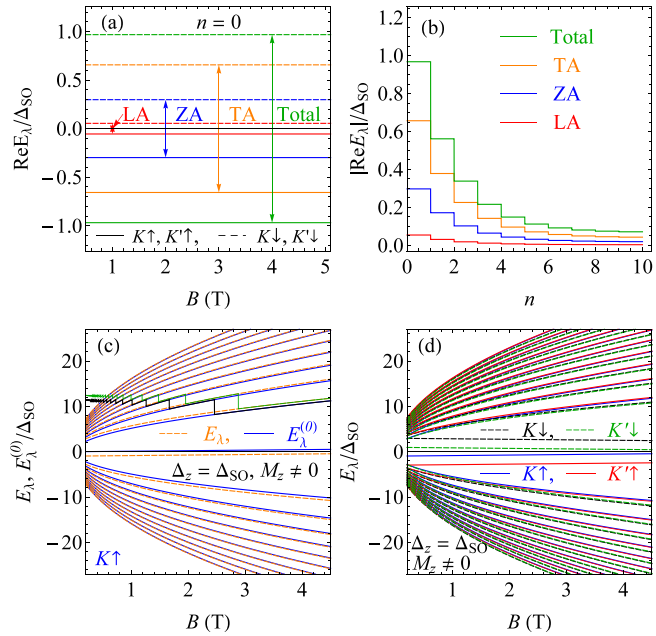

FIG. 1. The exchange self-energy corrections and the splitting of energy levels: The real part of the exchange self-energy versus the magnetic field for (a) $n = 0$ and (b) the Landau level. (c) The splitting of the energy level for $K\uparrow$ due to acoustic phonon interaction versus the magnetic field; the green and black curves show the chemical potential vs B with and without phonon corrections, respectively. (d) The dependence of E_λ on the magnetic field. In all panels, the electron concentration is $n_e = 5 \times 10^{11}$ cm^{-2}, and $T = 2$ K.

been reported for graphene. For example, Zhou *et al.* [43] reported total energy resolutions of 25 and 35 meV, which were taken on single-layer epitaxial graphene at Beamline 12.0.1 and Beamline 7.0.1 of the Advanced Light Source of Lawrence Berkeley National Laboratory, respectively. The extraction of the real part of the self-energy $\mathrm{Re}\Sigma$ also showed a maximum value of about 20 meV (see Fig. 1(d) of Ref. [43]). In another work, Bianchi *et al.* [44] reported a maximum value of the real part of the self-energy due to electron-phonon scattering in potassium-doped graphene which amounted to over 40 meV. These values are larger than those in silicene (due to only acoustic phonons interaction) because in the experimental measurement the total contribution of many phonon branches (acoustic, optical, and surface phonons) has been taken into account. We also see that the correction using the self-energy due to electron-phonon scattering in graphene has been used widely and gives results close to the experimental data. For example, Pound *et al.* [45] found a result for the real part of the self-energy caused by electron-phonon scattering of about 15 meV. In another work, using Migdal approximation, Doğan and F. Marsiglio [46] found a result for the real part of the self-energy of about 10 meV. Although these results have been found in graphene, in the case of the absence of magnetic field and due to the total contribution of many phonon branches, roughly estimated, these values of the correction energy are the same order as those of our results for silicene using Migdal approximation. Moreover, in contrast to the situation in gapped graphene [22], where the energy correction value due to impurity scattering is much smaller than

the mass term Δ, in silicene, this correction (for the zero level) is equivalent to that of SOC strength. Therefore, the phonon correction makes a significant contribution to the correction of LL energy and therefore to the transport properties of silicene. For that reason, it is necessary to take this effect into account.

The phonon correction to the energy of different levels is exhibited in Fig. 1(b). One sees that the correction effect is strongest at the zero level and then gradually decreases at the higher LLs. For the levels with $n > 10$, the correction is very weak and can be neglected.

The LLs for the $K\uparrow$ case in silicene with (E_λ) and without ($E_\lambda^{(0)}$) phonon correction are shown in Fig. 1(c) for $\Delta_z = \Delta_{SO}$ and $M_z \neq 0$, (i.e., $M_z = e\hbar B/m_e$, which depends on the magnetic field B). The green and black curves present the chemical potential with and without phonon correction, respectively, which is inferred from the electron concentration n_e, given as

$$n_e = \int_{-\infty}^{+\infty} D(E)f(E)dE = \frac{1}{2\pi\alpha_c^2}\sum_{n,s,\tau,p} f_{n,s}^{\tau,p}, \tag{11}$$

where $D(E) = (1/\mathcal{S}_0)\sum_{n,s,\tau,p,k_y}\delta(E - E_{n,s}^{\tau,p})$ is the density of states and $f_{n,s}^{\tau,p} = f(E_{n,s}^{\tau,p}) = [\exp\beta(E_{n,s}^{\tau,p} - \mu) + 1]^{-1}$. When the phonon correction effect is taken into account, the LLs are modified, leading to the change in n_F (n_F is the largest value of the occupied LL). This results in different steps in the chemical potential between the cases with and without the phonon correction effect. The electric field value of $\Delta_z = \Delta_{SO}$ is taken to repeal the SOC term for the $K\uparrow$ case (and for the $K'\downarrow$ case as well), leading its LLs spectrum to those of graphene [24,27], called the graphene form of silicene. Meanwhile, the Zeeman field separates the LLs into two levels due to spin polarization. For the case of spin up shown in Fig. 1(c), the Zeeman field lifts the LLs. It is clear that the acoustic phonon correction contributes to the expansion of the silicene energy gap even in its graphene form.

The full picture of the LLs of silicene at $\Delta_z = \Delta_{SO}$ and $M_z \neq 0$ is shown in Fig. 1(d), where the phonon correction is included. The splitting of LLs into two components, for each valley, is clearly observed. In contrast to the case of $M_z = 0$ [25] where the LLs exhibit double valley degenerate feature, here, the presence of the Zeeman field splits the LLs and makes them nondegenerate. In addition, the opening energy gap induced by the phonon correction is valid in all cases of valleys and spins, making the silicene energy gap a finite value even in the case of its graphene form. It is noted that $\mathrm{Re}\Sigma_\lambda$ is also affected by a change in the electron concentration (see Appendix B). However, this influence is so weak that it has been ignored in this study.

IV. CONDUCTIVITIES AND RESISTIVITIES

A. Hall conductivity

According to the linear response theory presented in Ref. [47], the conductivity has two parts: diagonal and nondiagonal. Its full form is $\sigma_{\mu\nu} = \sigma_{\mu\nu}^d + \sigma_{\mu\nu}^{nd}$, with $\mu, \nu = x, y$. The nondiagonal part plays the role of the Hall conductivity, shown to be [21,22,25,48]

$$\sigma_{\mu\nu}^{nd} = \frac{ie^2\hbar}{\mathcal{S}_0}\sum_{\lambda\neq\lambda'}\frac{(f_\lambda - f_{\lambda'})v_{\lambda\lambda'}^{\nu}v_{\lambda'\lambda}^{\mu}}{(E_\lambda - E_{\lambda'})(E_\lambda - E_{\lambda'} + i\Gamma_\lambda)}. \tag{12}$$

The sum is taken over all quantum numbers of states $|\lambda\rangle = |\alpha, k_y\rangle$ and $|\lambda'\rangle = |\alpha', k_y'\rangle$ as long as $|\lambda\rangle \neq |\lambda'\rangle$, and Γ_λ refers to the LL broadening. Assuming that the LL broadening has the same value for all states, $\Gamma_\lambda \approx \Gamma = \gamma\hbar\omega_c \propto \sqrt{B}$ (γ is a dimensionless parameter), which is demonstrated to be proportional to the square root of the magnetic field [49], the imaginary part of Eq. (12) will be vanishing [22,25]. In this case, the denominator in Eq. (12) can be replaced by $(E_\lambda - E_{\lambda'})^2 + \Gamma^2$ (see Appendix C). In the following, we mainly take $\Gamma = 0$ to obtain the apparent expression for the Hall conductivity σ_{yx}. The finite values of Γ ($\Gamma \neq 0$) will be considered an extra result of the Hall conductivity to contrast with that for $\Gamma = 0$ (see Fig. 10 and the related discussion in Appendix C).

In Eq. (12), $v_{\lambda\lambda'}^{v=x} = \langle\lambda|v_x|\lambda'\rangle$ and $v_{\lambda'\lambda}^{\mu=y} = \langle\lambda'|v_y|\lambda\rangle$ are the velocity matrix elements, their product for the K valley ($\tau = +$), $\mathcal{P}_{\{nn'\}}^K = v_{\lambda\lambda'}^{x,K}v_{\lambda'\lambda}^{y,K}$, is given as follows for $\mu = y$ and $\nu = x$:

$$\mathcal{P}_{\{nn'\}}^K = iv_F^2\delta_{k_y,k_y'}\delta_{s,s'}\left[\left|A_{n,s}^{+,p}B_{n',s'}^{+,p'}\right|^2\delta_{n',n-1} - \left|A_{n',s'}^{+,p'}B_{n,s}^{+,p}\right|^2\delta_{n',n+1}\right], \tag{13}$$

where we have used the general formula $\mathbf{v} = \partial\mathcal{H}_0/\partial\mathbf{p}$, i.e., $v_x = v_F\sigma_x$ and $v_y = v_F\sigma_y$. Equation (13) indicates that the allowed transitions from n-LL to n'-LL satisfy the condition $n' = n \pm 1$ with the same spin indices and at the same k_y point. For transitions involving zero level, corresponding to Eq. (13), we have

$$\mathcal{P}_{\{0n'\}}^K = -\delta_{k_y,k_y'}\delta_{s,s'}iv_F^2\left(A_{n',s'}^{+,p'}\right)^2\delta_{0,n'-1}, \tag{14}$$

$$\mathcal{P}_{\{n0\}}^K = \delta_{k_y,k_y'}\delta_{s,s'}iv_F^2\left(A_{n,s}^{+,p}\right)^2\delta_{n-1,0}. \tag{15}$$

To obtain the expression for Hall conductivity we follow the procedure suggested by Krstajić and Vasilopoulos [22] as well as by Shakouri *et al.* [25], who found the Hall conductivity contributed from the K valley to be expressed as $\sigma_{yx}^K = \sigma^K + \delta\sigma^K$ for $n \geqslant 1$, with

$$\sigma^K = \frac{e^2}{2h}\sum_{n=1,s}(2n+1) \times (f_{n,s}^{+,+} - f_{n+1,s}^{+,+} + f_{n,s}^{+,-} - f_{n+1,s}^{+,-}), \tag{16}$$

$$\delta\sigma^K = \frac{e^2}{2h}\sum_{n=1,s}\Delta_{+,s}^z \times \left(\frac{f_{n+1,s}^{+,+} - f_{n+1,s}^{+,-}}{E_{n+1,s}^+} - \frac{f_{n,s}^{+,+} - f_{n,s}^{+,-}}{E_{n,s}^+}\right). \tag{17}$$

The corresponding expression for $n = 0$ is

$$\sigma_{yx}^{0K} = \frac{e^2}{2h}\sum_{s=\pm}\frac{1}{E_{1,s}^+}[2E_{1,s}^+f_{0,s} - E_{1,s}^+(f_{1,s}^{+,+} + f_{1,s}^{+,-}) + \Delta_{+,s}^z(f_{1,s}^{+,+} - f_{1,s}^{+,-})]. \tag{18}$$

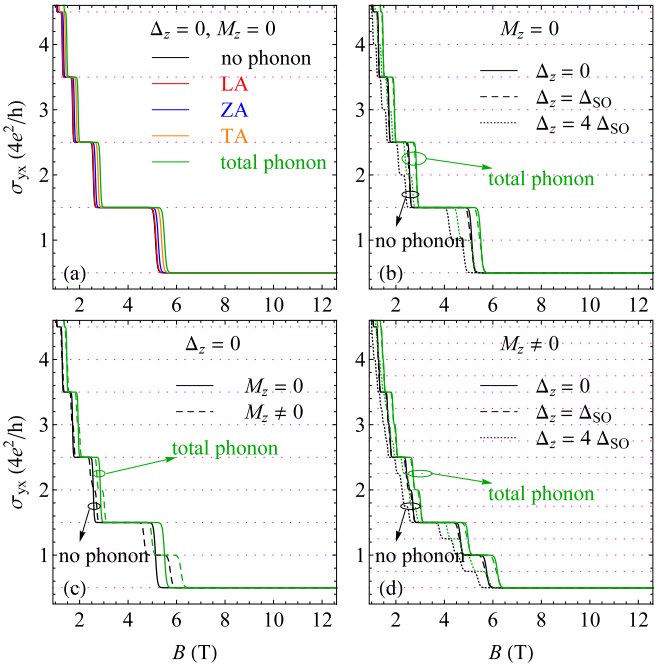

FIG. 2. Hall conductivity as a function of magnetic field with and without phonon corrections at different values of Δ_z and M_z: (a) $\Delta_z = 0$, $M_z = 0$, (b) $\Delta_z \neq 0$, $M_z = 0$, (c) $\Delta_z = 0$, $M_z \neq 0$, and (d) $\Delta_z \neq 0$, $M_z \neq 0$. The electron concentration is $n_e = 5 \times 10^{11}$ cm^{-2}, and $T = 2$ K.

The respective expressions for the contribution from the K' valley are $\sigma_{yx}^{K'} = \sigma^{K'} + \delta\sigma^{K'}$ and $\sigma_{yx}^{0K'}$, where $\sigma^{K'}$, $\delta\sigma^{K'}$, and $\sigma_{yx}^{0K'}$ have the same form as Eqs. (16), (17), and (18), respectively, but with $\Delta_{+,s}^{z}$ replaced by $-\Delta_{-,s}^{z}$ wherever it appears. Since $\Delta_{+,\pm}^{z} = \Delta_{-,\mp}^{z}$, the terms $\Delta_{\tau,s}^{z}$ cancel each other when summing over spin and valley contributions. Consequently, the Hall conductivity due to the total contribution of the two valleys and spins, $\sigma_{yx} = \sigma_{yx}^{K} + \sigma_{yx}^{K'}$, is then calculated as follows:

$$\sigma_{yx} = \frac{e^2}{2h}\sum_{\tau,s}\Big\{\big[2f_{0,s}^{\tau} - \big(f_{1,s}^{\tau,+} + f_{1,s}^{\tau,-}\big)\big] + \sum_{n=1}(2n+1) \times \big(f_{n,s}^{\tau,+} - f_{n+1,s}^{\tau,+} + f_{n,s}^{\tau,-} - f_{n+1,s}^{\tau,-}\big)\Big\}. \quad (19)$$

Equation (19) has the same form as that obtained in Ref. [25] for silicene, except for the influences of the Zeeman field and the phonon corrections to the LLs, which were neglected in that previous study. Although the Hall conductivity does not explicitly depend on $\Delta_{\tau,s}^{z}$, the size of the band gap still affects σ_{yx} through its presence in the expression for the energy spectrum, which strongly affects the Fermi distribution function $f_{n,s}^{\tau,p}$, as shown in Fig. 2.

In Fig. 2, the Hall conductivity versus magnetic field is shown for the cases with and without phonon corrections at different values of Δ_z and M_z at fixed electron concentration $n_e = 5 \times 10^{11}/\text{cm}^2$ and $T = 2$ K, which are chosen to compare with those reported in a previous work [25]. The roles of different acoustic phonon modes in the Hall conductivity are shown in Fig. 2(a). In comparison to the case without phonon correction, when the correction to the LLs due to the acoustic phonon is included, the QHE plateaus occur at higher values of the magnetic field because the phonon correction effect pushes the chemical potential up, as illustrated clearly in Fig. 1(c). Although the phonon correction effect also pushes the LLs up [see Fig. 1(c)], this effect on the chemical potential is stronger; therefore, the QHE plateaus in the case with the presence of phonon corrections occur in the higher magnetic field region in comparison to the case without phonon correction. This phononic shift is the weakest for the LA phonon, followed by that of the ZA one, while the TA phonon displays the strongest shift. The green curve is for the total effect of acoustic phonons, which will be used to present the phonon correction case in Figs. 2(b)–2(d). In addition, in the case of $\Delta = 0$ and $M_z = 0$ [Fig. 2(a)], each LL, except for the 0LL, has quadruple spin and valley degeneracy, and the QHE plateaus correspond to a half-integer, with the first one occurring at $2e^2/h$ and the sequence being $(4e^2/h)(n + 1/2)$. The fact that the QHE plateaus do not correspond to the conventional form $\sigma_{yx} = (4e^2/h)n$ but have an additional factor of $1/2$ is the sign of the anomalous integer QHE, which has been observed in graphene in both experiment [18,19,50] and theory [20–22,51,52] and in silicene [25].

In the case of $\Delta_z \neq 0$ and $M_z = 0$, i.e., when the electric field is included [see Fig. 2(b)], each LL is separated into two, reducing the degree of degeneracy from 4 to 2. As a result, the number of transitions is doubled, leading to the new steps in the Hall conductivity with the series being changed to $(4e^2/h)(n/2 + 1/2)$. The results are valid for cases both with and without phonon corrections, where the larger the electric field strength is, the clearer the separation is.

The effect of the Zeeman field on the Hall conductivity is shown in Fig. 2(c). Like in the case of $\Delta_z \neq 0$ and $M_z = 0$ displayed in Fig. 2(b), in this case, each LL is also double degenerate but for the valley index (i.e., $K\uparrow = K'\uparrow$ and $K\downarrow = K'\downarrow$). Consequently, the sequence of $(4e^2/h)(n/2 + 1/2)$ is also observed in the case of $\Delta_z = 0$ and $M_z \neq 0$. Interestingly, in comparison to the influence of the electric field, the effect of the Zeeman field is stronger. Therefore, the influence of this term should not be neglected in studying the QHE in silicene and 2D monolayer materials, in general.

A full picture of the combined effects of electric and Zeeman fields on the Hall conductivity is shown in Fig. 2(d). The LLs are completely separated or nondegenerate [see Fig. 1(d)], leading to the number of transitions being doubled in comparison to the cases for each individual effect in Figs. 2(b) and 2(c) or quadrupled in comparison to the case without both electric and Zeeman fields, i.e., $\Delta_z = 0$ and $M_z = 0$, as shown in Fig. 2(a). Consequently, new steps in the Hall conductivity are added, with the new sequence being found as $\sigma_{yx} = (4e^2/h)(n/4 + 1/2)$ both with and without phonon corrections. This series is different from that obtained in previous work [25], where the effect of the Zeeman field was not taken into account. Note that the additional factor of $1/2$ remains in all four cases, revealing that the anomalous integer-QHE feature in silicene is universal and independent of the influence of the electric and Zeeman fields.

In Fig. 3, the Hall conductivity of silicene is shown as a function of electron concentration for fixed magnetic field and temperature. The effect of different acoustic phonons on σ_{yx} is shown in Fig. 3(a), where the LA (ZA) phonon gives the

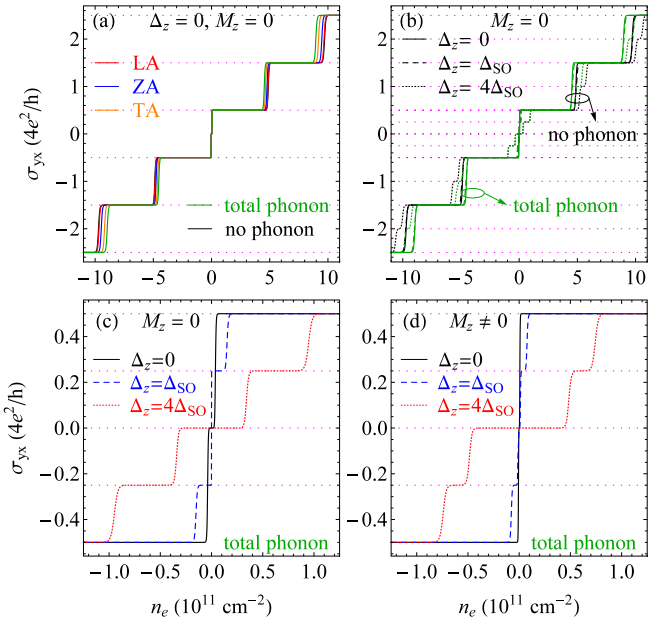

FIG. 3. Hall conductivity as a function of electron concentration n_e at $B = 5$ T and $T = 2$ K: (a) for different types of acoustic phonons at $\Delta_z = 0, M_z = 0$, (b) with and without phonon corrections for $M_z \neq 0$ at different values of Δ_z, (c) with phonon correction for $M_z = 0$ at different values of Δ_z, and (d) the same as in (c), but for $M_z \neq 0$.

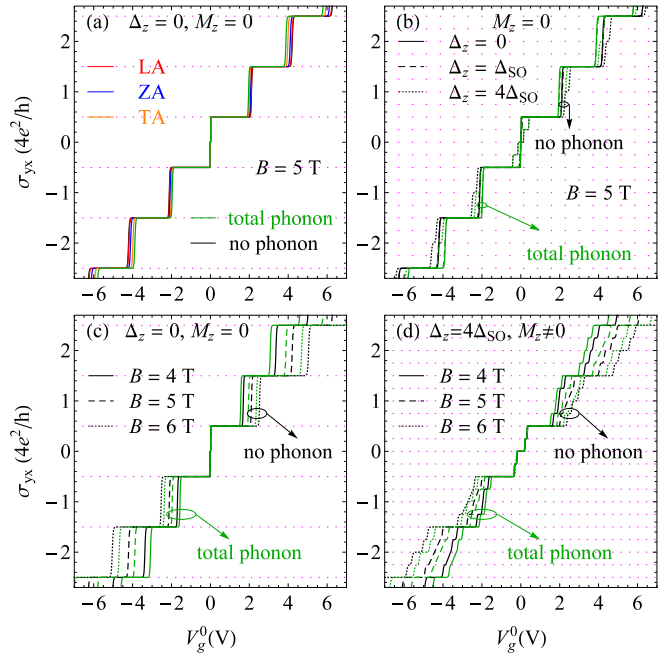

FIG. 4. Hall conductivity as a function of the applied voltage V_g^0 with and without phonon corrections at $T = 2$ K: (a) for $\Delta_z = 0$, $M_z = 0$, and $B = 5$ T with different types of acoustic phonons, (b) for $M_z = 0$ and $B = 5$ T at different values of Δ_z, (c) for $\Delta_z = 0, M_z = 0$ at different values of B, and (d) for $\Delta_z = 4\Delta_{SO}$, $M_z \neq 0$ at different values of B.

weakest (strongest) effect, as mentioned in Figs. 1 and 2. Figure 3(b) shows that when the phonon correction is included, the smaller value of n_e is needed to fill in the next LL. In addition, when the applied electric field is included, the new steps in σ_{yx} are found for both cases with and without phonon correction. Figure 3(c) shows the interesting results from the contribution of the zeroth level for $M_z = 0$ at different values of Δ_z. For $\Delta_z = \Delta_{SO}$ (blue dashed curve), the Hall conductivity shows ordinary behavior, similar to that of graphene [18,53]. This can be explained as follows: In the case of $\Delta_z = \Delta_{SO}$, the system displays the VSPM [9,13]; its SOC term for $K \uparrow$ and $K' \downarrow$ is canceled by the electric field [24], making the zeroth level (for $K \uparrow$ and $K' \downarrow$) in silicene degrade to that of graphene. Consequently, the Hall conductivity generated from $n = 0$ displays the usual behavior. The unusual additional plateaus at $\sigma_{yx} = \pm(e^2/h)$ are derived from $K \downarrow$ and $K' \uparrow$. Meanwhile, for the cases with $\Delta_z = 0$ (the topological insulator phase) and $\Delta_z = 4\Delta_{SO}$ (the band insulator phase) [9,13], there is an additional plateau at $\sigma_{yx} = 0$ in each curve, in agreement with experimental [54] and theoretical [22] results reported for graphene on a hexagonal boron nitride (h-BN) substrate as well as the theoretical result for silicene (without phonon correction) [26]. Figure 3(d) shows the same plots as in Fig. 3(c), but for $M_z \neq 0$. It is seen that when the Zeeman field is included ($M_z \neq 0$), the usual behavior disappears, and the Hall conductivity depicts unusual additional plateaus at $\sigma_{yx} = 0$ in all three phases (VSPM, TI, BI) of silicene.

It is noted that, when the silicene sample is performed on a substrate, for example, Al_2O_3, the electron concentration can be controlled by an applied voltage V_g^0 [55] due to their linear relation $n_e = \epsilon_s \epsilon_0 V_g^0/(e\ell)$ [18], where $\ell = 300$ nm is the substrate thickness and $\epsilon_s = 12.53$ [56] and ϵ_0 are the permittivities of the substrate and vacuum, respectively. In Fig. 4, the Hall conductivity is plotted versus the applied voltage V_g^0 at $T = 2$ K. Because of the linear relation between n_e and V_g^0, the behavior of σ_{yx} shown in Figs. 4(a) and 4(b) is the same as that obtained in Figs. 3(a) and 3(b), respectively. In Figs. 4(c) and 4(d), we show σ_{yx} versus the applied voltage for three values of the magnetic field both with and without phonon correction. It is seen that when the magnetic field increases the higher applied voltage is needed to create the next plateau. This happens with or without phonon correction, electric field, and Zeeman fields.

The additional plateaus in the Hall conductivity are also found to be dependent on the temperature: the plateau width becomes narrower when the temperature increases, agreeing with the result reported in a previous work [25] for silicene without the influence of the phonon correction. If we continue to increase the temperature, over 10 K, for example, the additional plateaus will be blurred away or may disappear even in the BI phase of silicene. This is the result of the fact that at high temperature, the thermal broadening of the Fermi distribution functions will become larger than the spacing between the LLs due to the extra contribution of electric and Zeeman fields. Figure 5(b) shows clearly that at the high temperature the additional plateaus induced by electric and Zeeman fields disappear because of the thermal broadening.

The dependence on the spin (s) and valley (τ) indexes of the Hall conductivity shown in Eqs. (16), (17), and (18) allows us to obtain the spin- (σ_{yx}^s) and valley- (σ_{yx}^τ) Hall

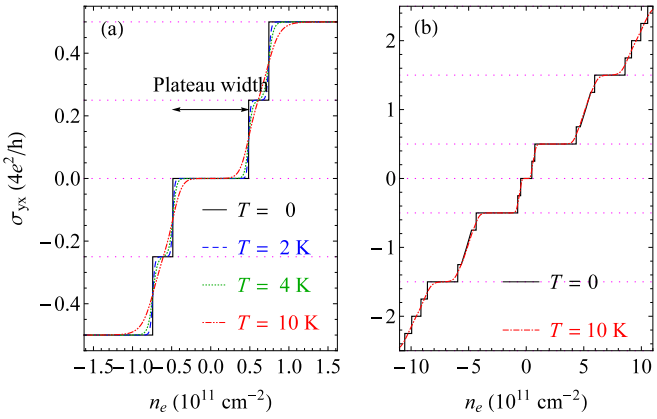

FIG. 5. Hall conductivity versus the electron concentration for different temperatures at $B = 5$ T, $\Delta_z = 4\Delta_{\rm SO}$, and $M_z \neq 0$. (a) and (b) are different only in the range of the axes.

conductivities, which are given as follows [15,57,58]:

$$\sigma_{yx}^{s} = \sigma_{yx}^{K\uparrow} - \sigma_{yx}^{K\downarrow} + \sigma_{yx}^{K'\uparrow} - \sigma_{yx}^{K'\downarrow}, \tag{20}$$

$$\sigma_{yx}^{\tau} = \sigma_{yx}^{K\uparrow} + \sigma_{yx}^{K\downarrow} - \sigma_{yx}^{K'\uparrow} - \sigma_{yx}^{K'\downarrow}. \tag{21}$$

Unlike in the expression for the Hall conductivity shown in Eq. (19), in the expressions for σ_{yx}^{s} and σ_{yx}^{τ} shown in Eqs. (20) and (21), the term $\Delta_{\tau,s}^{z}$ is not canceled. Therefore, the SOC term and the electric field have significant effects on these two types of Hall conductivities. In Fig. 6, we show σ_{yx}^{s} and σ_{yx}^{τ} versus the electric field both with and without phonon correction at $B = 5$ T and $T = 2$ K. Both σ_{yx}^{s} and σ_{yx}^{τ} are sensitive to the change in the electric field. Therefore, it is possible to

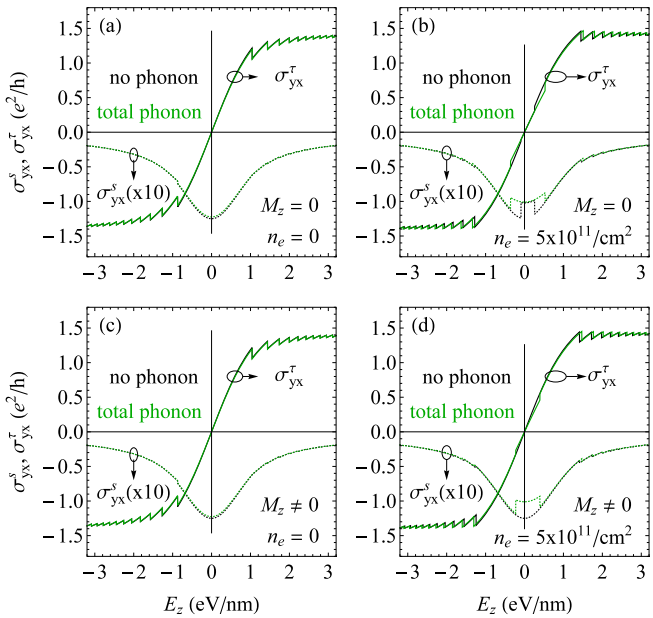

FIG. 6. Spin- and valley-Hall conductivities versus the perpendicular electric field E_z both with and without phonon corrections at $B = 5$ T and $T = 2$ K. (a) $M_z = 0$ and $n_e = 0$, (b) $M_z = 0$ and $n_e = 5 \times 10^{11}$ cm^{-2}, (c) $M_z \neq 0$ and $n_e = 0$, and (d) $M_z \neq 0$ and $n_e = 5 \times 10^{11}$ cm^{-2}.

use an electric field to tune the spin- and valley-Hall conductivities. The results obtained here are in qualitative agreement with those obtained in silicene in the absence of the magnetic field [15,57] except for the new transition steps observed in our work, where the magnetic field is included. In comparison to the case of $n_e = 0$ [Figs. 6(a) and 6(c)], i.e., the chemical potential is in the gap, when μ is in the conduction band [Figs. 6(b) and 6(d)], the transitions are more abundant due to the additional contributions of the intraband transitions. When $E_z = 0$, since the contributions to the Hall conductivity of the two spin states in each valley are equal but opposite, leading to the fact that $\sigma_{yx}^{K\uparrow} + \sigma_{yx}^{K\downarrow} = 0$ and $\sigma_{yx}^{K'\uparrow} + \sigma_{yx}^{K'\downarrow} = 0$, the valley-Hall conductivity is equal to zero in this case. Meanwhile, the spin-Hall conductivity is maximized at this value. In contrast, at large values of the electric field, the spin-Hall conductivities are reduced to zero, while the valley-Hall conductivities reach their saturation values in cases both with and without phonon corrections. In addition, since the phonon corrections to each individual conductivity ($\sigma_{yx}^{K\uparrow}$, $\sigma_{yx}^{K\downarrow}$, $\sigma_{yx}^{K'\uparrow}$, $\sigma_{yx}^{K'\downarrow}$) are nearly the same, they almost cancel each other one by one. Consequently, the spin- and valley-Hall conductivities evaluated by Eqs. (20) and (21) (shown in Fig. 6) are less sensitive to the phonon corrections than the usual Hall conductivity (shown in Figs. 2–4), whose total corrections are not canceled and are approximately considered to be quadruple that of each individual conductivity.

B. Longitudinal conductivity and resistivities

In general, both diffusion and collision mechanisms contribute to the current. In the magnetic field the diffusion vanishes; therefore, we evaluate only the longitudinal conductivity $\sigma_{xx}^{d} = \sigma_{xx}$ ($\mu = \nu = x$) caused by the hopping or the collision. It is given by [22,25,47]

$$\sigma_{xx} = \frac{e^2\beta}{2\mathcal{S}_0} \sum_{\lambda\lambda'} f(E_\lambda)[1 - f(E_{\lambda'})]\mathcal{W}_{\lambda'\lambda}(x_\lambda - x_{\lambda'})^2, \tag{22}$$

where $\beta = 1/(k_B T)$ and $x_\lambda = \langle\lambda|x|\lambda\rangle = \alpha_c^2 k_y$ is the orbit center matrix element. The transition rate for elastic impurity scattering can be expressed as follows:

$$\mathcal{W}_{\lambda'\lambda} = \frac{2\pi N_i}{\hbar \mathcal{S}_0} \sum_{q} |U(q)|^2 |J_{\lambda'\lambda}(u)|^2 \delta(E_{\lambda'} - E_\lambda)\delta_{k'_y, k_y \pm q_y}, \tag{23}$$

where $U(q) = U_0/(q^2 + q_s^2)^{1/2}$ is the Fourier transform of the impurity potential [24,59], with $q_s = 10^9$ m^{-1} being the screening wave vector. Here, $U_0 = e^2/(2\epsilon_0\epsilon)$, with $\epsilon = 4.0$ being the relative permittivity of silicene [24,60]. In Eq. (23), N_i is the impurity density. For the elastic impurity scattering, the only allowed transitions is $n \to n$; therefore, the corresponding form factors are given as follows:

$$|J_{\lambda\lambda}(u)|^2 = e^{-u}\left[\left|A_{n,s}^{\tau,p}\right|^2 L_{n-1}(u) + \left|B_{n,s}^{\tau,p}\right|^2 L_n(u)\right]^2. \tag{24}$$

Using Eq. (24) and then inserting Eq. (23) into Eq. (22), we have

$$\sigma_{xx} = \frac{e^2}{h} \frac{\beta N_i U_0^2}{4\hbar\omega_c} \sum_{n,s,\tau,p} K_{n,s}^{\tau,p} f\left(E_{n,s}^{\tau,p}\right)\left[1 - f\left(E_{n,s}^{\tau,p}\right)\right], \tag{25}$$

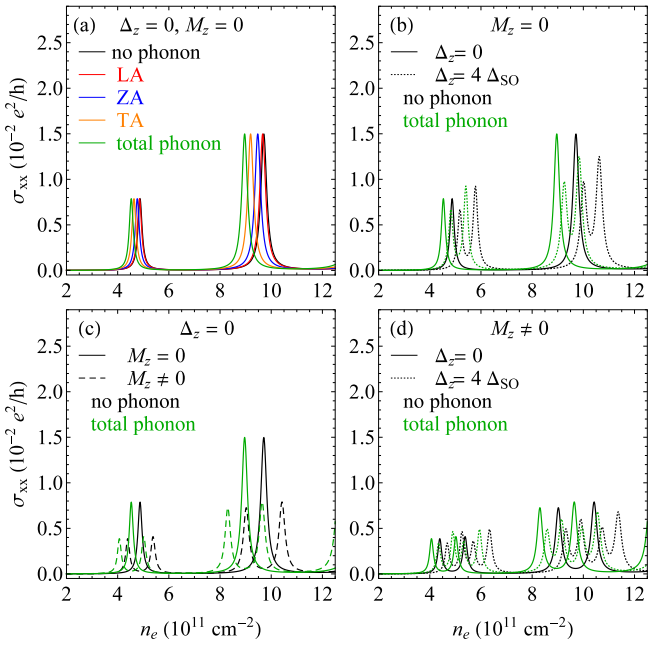

FIG. 7. The longitudinal conductivity versus the electron concentration for $N_i = 1.3 \times 10^9$ cm^{-2}, $B = 5$ T, and $T = 2$ K: (a) for different types of acoustic phonons at $\Delta_z = 0$ and $M_z = 0$, (b) with and without phonon correction for $M_z = 0$ at different values of Δ_z, (c) with and without phonon correction for $\Delta_z = 0$ at different values of M_z, and (d) the same as in (b), but for $M_z \neq 0$.

where

$$K_{n,s}^{\tau,p} = \int_0^\infty \frac{u}{u + b_s} |J_{\lambda\lambda}(u)|^2 du, \tag{26}$$

with $b_s = \alpha_c^2 q_s^2/2$. In the case of short-range scattering [22,25], we can expand $(u + b_s)^{-1}$ in the power of u/b_s [61], and

$$K_{n,s}^{\tau,p} = \sum_j (-1)^{j+1} \frac{K(j)}{b_s^j}, \quad j = 1, 2, 3, \ldots, \tag{27}$$

where

$$K(j) = \int_0^\infty u^j |J_{\lambda\lambda}(u)|^2 du. \tag{28}$$

For the first two values of j ($j = 1, 2$), the results are

$$K(1) = (2n-1)\left|A_{n,s}^{\tau,p}\right|^4 - 2n\left|A_{n,s}^{\tau,p}\right|^2\left|B_{n,s}^{\tau,p}\right|^2 + (2n+1)\left|B_{n,s}^{\tau,p}\right|^4, \tag{29}$$

$$K(2) = [2 + 6n(n-1)]\left|A_{n,s}^{\tau,p}\right|^4 - 8n^2\left|A_{n,s}^{\tau,p}\right|^2\left|B_{n,s}^{\tau,p}\right|^2 + [2 + 6n(n+1)]\left|B_{n,s}^{\tau,p}\right|^4. \tag{30}$$

In the limiting case, one can neglect the high-order terms ($j \geqslant 2$) and keep only one value, $j = 1$. The quantity $K_{n,s}^{\tau,p}$ in Eq. (27) then contains only one value of $K(1)$, which is shown in Eq. (29); the present result therefore reduces to that of Shakouri *et al.* [25].

In Fig. 7 we show the longitudinal conductivity σ_{xx}, given by Eq. (25) as a function of the electron concentration. The effect of different acoustic phonons on the longitudinal conductivity is shown in Fig. 7(a). One can see that when the phonon correction is taken into account, the peaks are shifted to the low-electron-concentration region. This shifting effect is strongest for the TA phonon, followed by that of the ZA phonon, and the LA phonon presents the weakest shift. This result is in agreement with what happened for the Hall conductivity shown in Fig. 3(a), where we report that when the phonon correction is included, the smaller value of electron concentration is needed to fill in the next LL, leading to the emergence of the next plateau in σ_{yx} and the peak in σ_{xx}. The appearance of the peaks of longitudinal conductivity can be understood analytically as follows. At low temperatures, in Eq. (25), one can use the relation $\beta f(E_{n,s}^{\tau,p})[1 - f(E_{n,s}^{\tau,p})] \approx \delta(\mu - E_{n,s}^{\tau,p})$ [23]; then broadening the δ function by the Lorentzian representation, i.e., $\delta(x) \to (\Gamma_1/\pi)(\Gamma_1^2 + x^2)$ [62], we obtain the expression for the longitudinal conductivity, which exhibits peaks wherever the condition $E_{n,s}^{\tau,p} = \mu$ is satisfied. It is clear that at a certain value of the magnetic field ($B = 5$ T, for example), the value of n_e (which satisfies the above condition) in the presence of phonon correction is smaller than that in the case without phonon correction. This fact helps us to understand the reason why the peaks in the longitudinal conductivity appear in the low region of the electron concentration when the phonon correction is included. The separate effects of the electric and Zeeman fields are presented in Figs. 7(b) and 7(c), respectively. One can see that both electric and Zeeman fields double the peaks of σ_{xx}. These results are similar to the double-plateau behavior of the Hall conductivity shown in Figs. 2(b) and 2(c), which is explained by the twofold degeneracy of the LLs due to the effect of the electric and Zeeman fields, respectively [27]. The double-peak behavior due to electric field is in agreement with a previous work [25], which reported the case without phonon correction. However, this result is valid in the case with the presence of the phonon correction as well. In Fig. 7(d) the combined effect of the electric and Zeeman fields has quadrupled the peaks of σ_{xx}, similar to the quadruple-plateau behavior of σ_{yx} shown in Fig. 2(d). This result is different from that found in previous works for graphene [18] and in silicene samples [25].

In this work, we also study the longitudinal and Hall resistivities, which can be expressed through their corresponding conductivities by

$$\rho_{xx} = \sigma_{xx}/S, \quad \rho_{xy} = \sigma_{yx}/S, \tag{31}$$

where $S = \sigma_{xx}^2 + \sigma_{yx}^2$. The results for the longitudinal and Hall resistivities are exhibited in Fig. 8. It is seen from all four panels that the peaks of ρ_{xx}, which are found to appear in a series presenting the Shubnikov–de Haas oscillation (SdHO), correspond to the transition points between the plateaus of ρ_{xy}. This is a typical feature, as reported in several two-dimensional materials such as graphene [18,22,50,63], silicene [25], and the MoS_2 monolayer [23]. In detail, Fig. 8(a) shows the dependence of the resistivities on the electron concentration for different types of acoustic phonons at $\Delta_z = M_z = 0$. Similar to the results for the conductivities shown in Figs. 3(a) and 7(a), the effect of the TA phonon on the resistivities is also found to be the strongest, followed by that of the ZA phonon, while the LA phonon displays the weakest effect. For the Hall

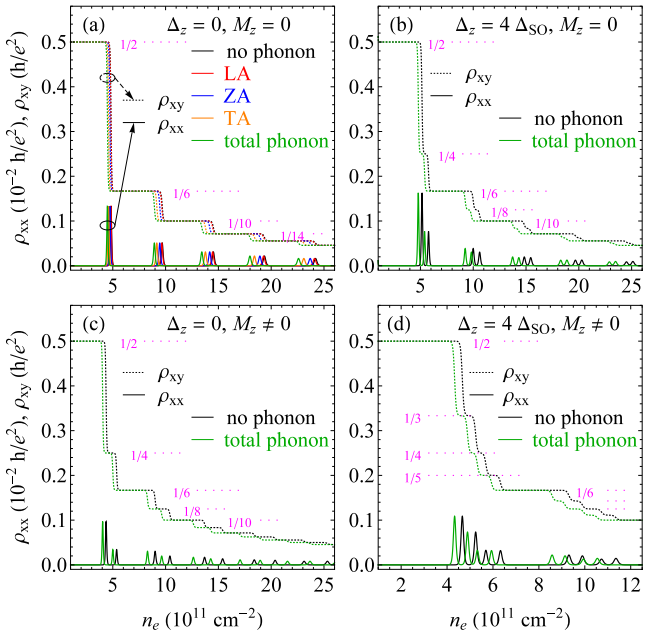

FIG. 8. The Hall, ρ_{xy}, and longitudinal, ρ_{xx}, resistivities versus the electron concentration for $N_i = 1.3 \times 10^9$ cm^{-2}, $B = 5$ T, and $T = 2$ K: (a) for different types of acoustic phonons at $\Delta_z = 0$ and $M_z = 0$, (b) with and without phonon correction for $M_z = 0$ and $\Delta_z = 4\Delta_{SO}$, (c) with and without phonon correction for $\Delta_z = 0$ and $M_z \neq 0$, and (d) the same as in (b), but for $M_z \neq 0$.

resistivity, the height of its plateau in this case ($\Delta_z = M_z = 0$) is found to appear in the sequence of $(h/e^2)/[2(2n+1)]$, with $n = 0, 1, 2, \ldots$. The separate effects of the electric and Zeeman fields on the resistivities are presented in Figs. 8(b) and 8(c), respectively. Like for the cases of the conductivities shown in Figs. 7(b) and 7(c), here, we also find that both electric and Zeeman fields double the peaks of the SdHO of the longitudinal resistivity. The double-peak behavior of the longitudinal resistivity was experimentally observed in graphene on an h-BN substrate [50], and we hope that a similar observation will be possible in silicene. The corresponding heights of the plateaus in these cases are found to appear in the series of $(h/e^2)/[2(n+1)]$, in agreement with that reported in previous work [25]. Finally, the combined effect of the electric and Zeeman fields on the resistivities is shown in Fig. 8(d). One can see that this combined effect quadruples the peaks of ρ_{xx} and leads to the sequence of $(h/e^2)/(n+2)$ in the height of the plateaus in ρ_{xy}. This quadruple peak and the sequence of $(h/e^2)/(n+2)$ features have not been found in graphene [19,63] or in silicene where the Zeeman field effect was ignored [25].

V. SUMMARY

We studied the quantum magnetotransport properties of silicene when the acoustic phonon correction to the LL energy is included. Since the phonon interaction is found to have a significant contribution to the correction of the LLs, it has a remarkable effect on the transport properties of silicene. The strongest effect is induced by the TA phonon, followed by that of the ZA phonon, and the LA phonon shows the weakest effect. In the case of $\Delta = 0$ and $M_z = 0$, the quadruple spin and valley degeneracy feature lead to the QHE plateaus corresponding to a half-integer with the sequence $(4e^2/h)(n+1/2)$. The separate effects of electric and Zeeman fields reduce the degree of degeneracy to 2, leading to the double plateau in the Hall conductivity/resistivity as well as to the double peak in the longitudinal conductivity/resistivity. The combined effect of the electric and Zeeman fields makes the LLs completely separate (nondegenerate), which is the cause of the unusual additional plateaus at $\sigma_{yx} = 0$ in all three phases (VSPM, TI, BI) of silicene, leading to the QHE plateaus corresponding to the unusual sequence of $(4e^2/h)(n/4+1/2)$. It also leads to the quadruple plateau in the Hall conductivity/resistivity as well as to the quadruple peak of the SdHO of the longitudinal conductivity/resistivity.

Experimentally, a useful way to observe the QHE is to study the Hall conductivity versus the gate voltage. With increasing magnetic field, higher applied voltage is needed to build the next plateau. The temperature is found to have a significant effect on the width of the Hall conductivity plateaus. The best temperature region for observing the additional plateaus of the Hall conductivity is in the region lower than 10 K. In the higher-temperature region, the additional plateaus will fade or may disappear even in the BI phase of silicene. As far as the spin- and valley-Hall conductivities are concerned, we demonstrated that these features can be tuned by tuning the electric field: at an electric field value of zero (large), the valley-Hall conductivities are equal to zero (reach their saturation values), while the spin-Hall conductivity reaches its maximum value (reduces to zero). Finally, we addressed the quadruple peaks of ρ_{xx} and the sequence $(h/e^2)/(n+2)$ in the height of the plateaus in ρ_{xy} caused by the combined effect of the electric and Zeeman fields. These are the results of the complete nondegeneracy of the LLs. Our results provide useful data required in the experiments as well as research on spin- and valley-based electronic devices.

ACKNOWLEDGMENTS

This research is funded by the Vietnam National Foundation for Science and Technology Development (NAFOSTED) under Grant No. 103.01-2019.11.

APPENDIX A: ENERGY CORRECTION USING FIRST-ORDER PERTURBATION THEORY

1. Impurity scattering

The k_y correction to the LLs of the $|\lambda, k_y\rangle$ state due to scattering by screened Coulomb impurities is given by [21,22]

$$\Delta E_\lambda^{\rm im} = \langle \lambda, k_y | U(\mathbf{r}) | \lambda, k_y \rangle, \tag{A1}$$

where $U(\mathbf{r}) = (e^2/4\pi\epsilon_r\epsilon_0 r)e^{-k_s r}$ is the impurity potential. Using the procedure presented by Krstajić and Vasilopoulos [21] and formula (7.414.7) in Ref. [64], Eq. (A1) is found to be

$$\Delta E_\lambda^{\rm im} \approx \frac{U_0}{2\pi\alpha_c\sqrt{2b_s}}\left[I_n^{(0)} - \left(\varsigma^2 + \frac{1}{2b_s}\right)I_n^{(1)} + \frac{\varsigma^2}{2}\left(\frac{\varsigma^2}{3} + \frac{1}{b_s}\right)I_n^{(2)} - \frac{\varsigma^4}{12b_s}I_n^{(3)}\right], \tag{A2}$$

where $\varsigma = \alpha_c k_x$ and

$$I_n^{(\beta)} = \left(A_{np}^{\tau s}\right)^2 J_{n-1}^{(\beta)} + \left(B_{np}^{\tau s}\right)^2 J_n^{(\beta)}. \tag{A3}$$

Here,

$$J_n^{(\beta)} = \beta! 2^{\beta+1} {}_2F_1(-n, \beta+1; 1; 2), \tag{A4}$$

with ${}_2F_1(-n, \beta+1; 1; 2)$ being the hypergeometric functions. For the numerical calculation of $\Delta E_\lambda^{\rm im}$, the value of $k_x = 10^6$ m^{-1} is taken. At $B = 5$ T, $|\Delta E_n^{\rm im}|$ calculated in Eq. (A2) has values of $0.69\Delta_{\rm SO}$, $1.34\Delta_{\rm SO}$, $1.30\Delta_{\rm SO}$, $1.25\Delta_{\rm SO}$, and $1.21\Delta_{\rm SO}$, corresponding to values of 2.70, 5.23, 5.06, 4.89, and 4.72 meV, respectively, for the correction to the first five levels, i.e., $n = 0, 1, 2, 3, 4$.

2. Acoustic phonon scattering

The k_y correction to the LLs of the $|\lambda, k_y\rangle$ state due to scattering by acoustic phonons is as follows:

$$\Delta E_\lambda^{\rm ph} = \langle \lambda, k_y | U(\mathbf{r}) | \lambda, k_y \rangle, \tag{A5}$$

where $U(\mathbf{r}) = (1/S_0)\sum_{\mathbf{q}} U(q) e^{i\mathbf{q}\cdot\mathbf{r}}$ is the potential, with $U(q) = J_{\lambda\lambda}(u) g_q^\zeta$. Using the procedure presented in Ref. [21], we obtain

$$\Delta E_\lambda^{\rm ph,\pm} = \frac{D_a}{2\pi}\sqrt{\frac{\hbar}{2S_0\rho v_{s\lambda}}}\int_0^\infty q^{3/2} J_{\lambda\lambda}(u)\sqrt{N_{q,\zeta}^{\pm}}\, dq. \tag{A6}$$

Here, the plus (+) and minus (−) signs correspond to the processes of *emission* and absorption of phonons, respectively, and $N_{q,\zeta}^{\pm} = N_{q,\zeta} + 1/2 \pm 1/2$. For $B = 5$ T, Eq. (A6) gives the numerical values 0.018, 0.025, 0.029, 0.033, and 0.037 meV for the total correction to the first five levels. These values are much smaller than those calculated by the Migdal approximation used in the main text. As can see from Eq. (A5), in the perturbation theory, only the intra-LL interactions are allowed ($\lambda' = \lambda$). Meanwhile, in the Migdal approximation method, only the inter-LL interactions are allowed [see Eq. (7)], which leads to the fact that the estimate of the self-energy using the Migdal approximation is approximately two orders of magnitude larger than that using the first-order perturbation theory.

APPENDIX B: EFFECT OF THE ELECTRON CONCENTRATION ON THE SELF-ENERGY

In Fig. 9, we show the dependence of the real part of the exchange self-energy for $n = 0$ on the electron concentration. It is seen that $\mathrm{Re}\Sigma_\lambda$ decreases with the increase of n_e. However, in the entire range of n_e from 0.5×10^{11} to 25×10^{11} cm^{-2}, this reduction is so weak that $\mathrm{Re}\Sigma_\lambda$ can be seen to be independent of the change in the electron concentration.

APPENDIX C: HALL CONDUCTIVITY FOR $\Gamma \neq 0$

To obtain the Hall conductivity expression for the case with $\Gamma \neq 0$, we follow the procedure presented by Krstajić and Vasilopoulos [21]. From Eq. (12), assuming $\Gamma_\lambda = \Gamma$, multiplying and dividing by $E_\lambda - E_{\lambda'} - i\Gamma$, we have

$$\sigma_{\mu\nu}^{nd} = \frac{ie^2\hbar}{\mathcal{S}_0}\sum_{\lambda\neq\lambda'}\frac{(f_\lambda - f_{\lambda'})v_{\lambda\lambda'}^\nu v_{\lambda'\lambda}^\mu}{(E_\lambda - E_{\lambda'})^2 + \Gamma^2}. \tag{C1}$$

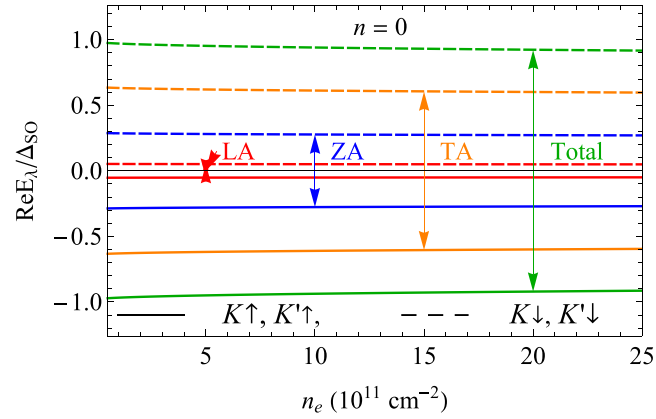

FIG. 9. The real part of the exchange self-energy versus the electron concentration for $n = 0$ at $B = 5$ T and $T = 2$ K.

From Eqs. (2) and (6) we see that the difference $E_\lambda - E_{\lambda'}$ is approximately of the order of the cyclotron energy $\hbar\omega_c$, i.e., $E_\lambda - E_{\lambda'} \approx \hbar\omega_c[1 - (\Delta_{\rm SO} - \Delta_z)^2/2(\hbar\omega_c)^2]$. For small Γ such that $\Gamma/\hbar\omega_c = \gamma \ll 1$, the denominator in Eq. (C1) can be expanded in powers of $\{\Gamma/\hbar\omega_c[1 - (\Delta_{\rm SO} - \Delta_z)^2/2(\hbar\omega_c)^2]\}^2 = \gamma^2/[1 - (\Delta_{\rm SO} - \Delta_z)^2/2(\hbar\omega_c)^2]^2$. Then, we have

$$\sigma_{\mu\nu}^{nd} \cong \frac{ie^2\hbar}{\mathcal{S}_0}\sum_{\lambda\neq\lambda'}\frac{(f_\lambda - f_{\lambda'})v_{\lambda\lambda'}^\nu v_{\lambda'\lambda}^\mu}{(E_\lambda - E_{\lambda'})^2}(1 - \eta^2), \tag{C2}$$

where η is a dimensionless parameter given as

$$\eta = \frac{\gamma}{1 - (\Delta_{\rm SO} - \Delta_z)^2/2(\hbar\omega_c)^2}. \tag{C3}$$

Equation (C2) reveals that the Hall conductivity for the case with $\Gamma \neq 0$ is the result of the product of σ_{yx} in Eq. (19) and $(1 - \eta^2)$. For $\Gamma = 0$ or $\eta = 0$, Eq. (C2) reduces to the usual expression of the Hall conductivity shown in Eq. (19).

In Fig. 10 we show the effect of LL broadening on the Hall conductivity (recalling that $\gamma = \Gamma/\hbar\omega_c$). We see that in the case with $\Gamma \neq 0$ the QHE plateaus shift downward and

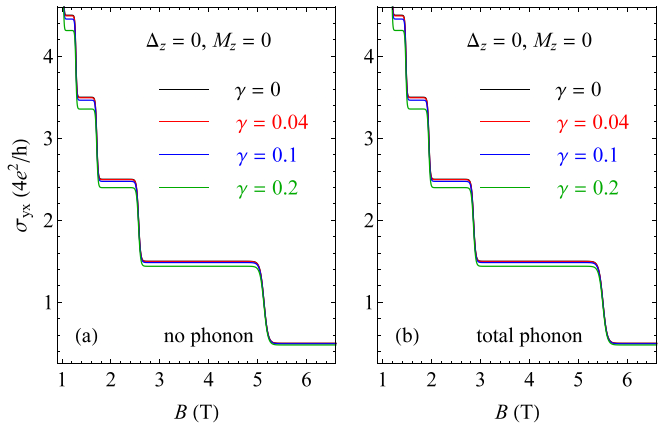

FIG. 10. Hall conductivity versus the magnetic field for different LL broadenings at $\Delta_z = 0$ and $M_z = 0$: (a) no phonon and (b) total phonon. The electron concentration is $n_e = 5 \times 10^{11}$ cm^{-2} and $T = 2$ K.

no longer correspond to a half-integer unlike in the case of $\Gamma = 0$ (the black line). The shifting is proportional to the magnitude of the LL broadening. However, this shifting is really weak, even at $\gamma = 0.2$ in cases both with and without phonon corrections. In the main text, we considered only the Hall conductivities for $\Gamma = 0$.

[1] K. Takeda and K. Shiraishi, Phys. Rev. B **50**, 14916 (1994).
[2] G. G. Guzmán-Verri and L. C. Lew Yan Voon, Phys. Rev. B **76**, 075131 (2007).
[3] S. Lebègue and O. Eriksson, Phys. Rev. B **79**, 115409 (2009).
[4] K. S. Novoselov, A. K. Geim, S. V. Morozov, D. Jiang, Y. Zhang, S. V. Dubonos, I. V. Grigorieva, and A. A. Firsov, Science **306**, 666 (2004).
[5] C.-C. Liu, W. Feng, and Y. Yao, Phys. Rev. Lett. **107**, 076802 (2011).
[6] C.-C. Liu, H. Jiang, and Y. Yao, Phys. Rev. B **84**, 195430 (2011).
[7] P. Vogt, P. De Padova, C. Quaresima, J. Avila, E. Frantzeskakis, M. C. Asensio, A. Resta, B. Ealet, and G. Le Lay, Phys. Rev. Lett. **108**, 155501 (2012).
[8] L. Meng, Y. Wang, L. Zhang, S. Du, R. Wu, L. Li, Y. Zhang, G. Li, H. Zhou, W. A. Hofer, and H.-J. Gao, Nano Lett. **13**, 685 (2013).
[9] M. Ezawa, Phys. Rev. Lett. **109**, 055502 (2012).
[10] Z. Ni, Q. Liu, K. Tang, J. Zheng, J. Zhou, R. Qin, Z. Gao, D. Yu, and J. Lu, Nano Lett. **12**, 113 (2012).
[11] N. D. Drummond, V. Zólyomi, and V. I. Fal'ko, Phys. Rev. B **85**, 075423 (2012).
[12] M. Ezawa, New J. Phys. **14**, 033003 (2012).
[13] C. J. Tabert and E. J. Nicol, Phys. Rev. B **88**, 085434 (2013).
[14] M. Ezawa, Phys. Rev. B **86**, 161407(R) (2012).
[15] M. Tahir, A. Manchon, K. Sabeeh, and U. Schwingenschlögl, Appl. Phys. Lett. **102**, 162412 (2013).
[16] K. v. Klitzing, G. Dorda, and M. Pepper, Phys. Rev. Lett. **45**, 494 (1980).
[17] K. von Klitzing, T. Chakraborty, P. Kim, V. Madhavan, X. Dai, J. McIver, Y. Tokura, L. Savary, D. Smirnova, A. M. Rey, C. Felser, J. Gooth, and X. Qi, Nat. Rev. Phys. **2**, 397 (2020).
[18] K. S. Novoselov, A. K. Geim, S. V. Morozov, D. Jiang, M. I. Katsnelson, I. V. Grigorieva, S. V. Dubonos, and A. A. Firsov, Nature (London) **438**, 197 (2005).
[19] Y. Zhang, Y.-W. Tan, H. L. Stormer, and P. Kim, Nature (London) **438**, 201 (2005).
[20] V. P. Gusynin and S. G. Sharapov, Phys. Rev. Lett. **95**, 146801 (2005).
[21] P. M. Krstajić and P. Vasilopoulos, Phys. Rev. B **83**, 075427 (2011).
[22] P. M. Krstajić and P. Vasilopoulos, Phys. Rev. B **86**, 115432 (2012).
[23] M. Tahir, P. Vasilopoulos, and F. M. Peeters, Phys. Rev. B **93**, 035406 (2016).
[24] K. Shakouri, P. Vasilopoulos, V. Vargiamidis, and F. M. Peeters, Phys. Rev. B **90**, 125444 (2014).
[25] K. Shakouri, P. Vasilopoulos, V. Vargiamidis, and F. M. Peeters, Phys. Rev. B **90**, 235423 (2014).
[26] M. Tahir and U. Schwingenschlögl, Sci. Rep. **3**, 1075 (2013).
[27] D. Muoi, N. N. Hieu, C. V. Nguyen, B. D. Hoi, H. V. Nguyen, N. D. Hien, N. A. Poklonski, S. S. Kubakaddi, and H. V. Phuc, Phys. Rev. B **101**, 205408 (2020).
[28] C.-H. Park, F. Giustino, M. L. Cohen, and S. G. Louie, Phys. Rev. Lett. **99**, 086804 (2007).
[29] E. H. Hwang and S. Das Sarma, Phys. Rev. B **87**, 115432 (2013).
[30] D. G. González, I. Zapata, J. Schiefele, F. Sols, and F. Guinea, Phys. Rev. B **96**, 125119 (2017).
[31] F. M. Peeters and J. T. Devreese, Phys. Rev. B **34**, 7246 (1986).
[32] T. Stauber and N. M. R. Peres, J. Phys.: Condens. Matter **20**, 055002 (2008).
[33] A. Pound, J. P. Carbotte, and E. J. Nicol, Phys. Rev. B **85**, 125422 (2012).
[34] B. Scharf, V. Perebeinos, J. Fabian, and I. Žutić, Phys. Rev. B **88**, 125429 (2013).
[35] B. Van Duppen, P. Vasilopoulos, and F. M. Peeters, Phys. Rev. B **90**, 035142 (2014).
[36] J. Menéndez, M. Noël, J. C. Zwinkels, and D. J. Lockwood, Phys. Rev. B **96**, 121201(R) (2017).
[37] F. Giustino, M. L. Cohen, and S. G. Louie, Nature (London) **452**, 975 (2008).
[38] C. M. Wang and X. L. Lei, Phys. Rev. B **87**, 235403 (2013).
[39] X. Li, J. T. Mullen, Z. Jin, K. M. Borysenko, M. Buongiorno Nardelli, and K. W. Kim, Phys. Rev. B **87**, 115418 (2013).
[40] E. H. Hwang and S. Das Sarma, Phys. Rev. B **77**, 115449 (2008).
[41] S. S. Kubakaddi and H. V. Phuc, Semicond. Sci. Technol. **36**, 025005 (2020).
[42] Z.-W. Wang, L. Liu, and Z.-Q. Li, Appl. Phys. Lett. **106**, 101601 (2015).
[43] S. Y. Zhou, D. A. Siegel, A. V. Fedorov, and A. Lanzara, Phys. Rev. B **78**, 193404 (2008).
[44] M. Bianchi, E. D. L. Rienks, S. Lizzit, A. Baraldi, R. Balog, L. Hornekær, and P. Hofmann, Phys. Rev. B **81**, 041403(R) (2010).
[45] A. Pound, J. P. Carbotte, and E. J. Nicol, Phys. Rev. B **84**, 085125 (2011).
[46] F. Doğan and F. Marsiglio, Phys. Rev. B **68**, 165102 (2003).
[47] M. Charbonneau, K. M. van Vliet, and P. Vasilopoulos, J. Math. Phys. **23**, 318 (1982).
[48] P. Vasilopoulos, Phys. Rev. B **32**, 771 (1985).
[49] Y. Zheng and T. Ando, Phys. Rev. B **65**, 245420 (2002).
[50] A. F. Young, C. R. Dean, L. Wang, H. Ren, P. Cadden-Zimansky, K. Watanabe, T. Taniguchi, J. Hone, K. L. Shepard, and P. Kim, Nat. Phys. **8**, 550 (2012).
[51] N. M. R. Peres, F. Guinea, and A. H. Castro Neto, Ann. Phys. (NY) **321**, 1559 (2006).
[52] N. M. R. Peres, F. Guinea, and A. H. Castro Neto, Phys. Rev. B **73**, 125411 (2006).
[53] Y. Zhang, Z. Jiang, J. P. Small, M. S. Purewal, Y.-W. Tan, M. Fazlollahi, J. D. Chudow, J. A. Jaszczak, H. L. Stormer, and P. Kim, Phys. Rev. Lett. **96**, 136806 (2006).
[54] C. R. Dean, A. F. Young, I. Meric, C. Lee, L. Wang, S. Sorgenfrei, K. Watanabe, T. Taniguchi, P. Kim, K. L. Shepard, and J. Hone, Nat. Nanotechnol. **5**, 722 (2010).

[55] A. H. Castro Neto, F. Guinea, N. M. R. Peres, K. S. Novoselov, and A. K. Geim, Rev. Mod. Phys. **81**, 109 (2009).

[56] B. Scharf, V. Perebeinos, J. Fabian, and P. Avouris, Phys. Rev. B **87**, 035414 (2013).

[57] S. Wang, P. Zhang, C. Ren, H. Tian, J. Pang, C. Song, and M. Sun, J. Supercond. Novel Magn. **32**, 2947 (2019).

[58] P. T. Huong, D. Muoi, H. V. Phuc, C. V. Nguyen, L. T. Hoa, B. D. Hoi, and N. N. Hieu, J. Mater. Sci. **55**, 14848 (2020).

[59] V. A. Margulis, J. Exp. Theor. Phys. **99**, 633 (2004).

[60] P.-H. Shih, Y.-H. Chiu, J.-Y. Wu, F.-L. Shyu, and M.-F. Lin, Sci. Rep. **7**, 40600 (2017).

[61] P. Vasilopoulos and C. M. Van Vliet, Phys. Rev. B **34**, 1057 (1986).

[62] Note that the quantity Γ_1 here is different from the term Γ in Eq. (12). Here, the quantity Γ_1 is used for the sole purpose of further explaining the occurrence of the peak of longitudinal conductivity at low temperatures. The results for σ_{xx} in Figs. 7 and 8 are plotted directly from Eq. (25), where the product $f(E^{\tau,p}_{n,s})[1 - f(E^{\tau,p}_{n,s})]$ has been used.

[63] C. R. Dean, A. F. Young, P. Cadden-Zimansky, L. Wang, H. Ren, K. Watanabe, T. Taniguchi, P. Kim, J. Hone, and K. L. Shepard, Nat. Phys. **7**, 693 (2011).

[64] A. Jeffrey and D. Zwillinger, *Table of Integrals, Series, and Products* (Elsevier, Amsterdam, 2007).